Journal of Alloys and Compounds 509 (2011) 5315–5319

Contents lists available at ScienceDirect

Journal of Alloys and Compounds

journal homepage: www.elsevier.com/locate/jallcom

Smart magnetodielectric nano-materials for the very high frequency applications

Atul Thakur[a], Preeti Thakur[b], Jen-Hwa Hsu[a,*]

[a] Department of Physics, National Taiwan University, 1 Roosevelt Road, Sec. 4, Taipei 106, Taiwan
[b] Physics Department, Himachal Pradesh University, Shimla 171005, India

ARTICLE INFO

Article history:
Received 11 October 2010
Received in revised form 30 January 2011
Accepted 1 February 2011
Available online 17 February 2011

Keywords:
Nanostructured materials
Precipitation
Sintering
Dielectric response
Ceramic
X-ray diffraction
Magnetization

ABSTRACT

Cobalt and copper doped Ni–Zn nano-ferrite with a composition of $Ni_{0.4}Zn_{0.4}Co_{0.2}Cu_{0.02}Fe_{1.98}O_4$ are prepared by a coprecipitation method. The structural, electromagnetic and magnetic properties are investigated by means of X-ray diffraction, impedance analyzer and vibrating sample magnetometer, respectively. Samples are calcinated at 600 °C and then subjected to different sintering temperatures. After sintering at 900 °C for 5 h, the average crystalline size is found to be 38 nm. The material shows almost constant permeability and permittivity, in the frequency range from 10 to 200 MHz, equal to ~10.8 (loss tangent ~ 0.04) and ~6.5 (loss tangent ~ 0.006), respectively. Relaxation phenomenon takes place beyond 200 MHz. The refractive index n is close to 8.3, and the reduced impedance Z/Z_0 is close to 1.3. The persistent and higher value of permeability than that of permittivity along with low losses enables this material useful for the very high frequency applications.

1. Introduction

Due to marvellous developments in wireless communication, demand for smaller and portable communication devices has always challenged the antenna designers. However, the support of various applications on a single channel makes the size of terminal physically bigger. There are many techniques for the patch antenna miniaturization. The popular technique is by using high permittivity substrates for antenna loading, but the return loss, bandwidth, impedance and gain of the antenna becomes worse and the efficiency of antenna is decreased [1]. The most important challenge is to reduce the physical dimensions of antenna without affecting the bandwidth and the electrical performance. Material dispersion (reduced bandwidth) and losses (reduced efficiency) are the crucial parameters to be controlled for antenna miniaturization. It has been reported that a substrate with lossless and dispersion-free permeability higher than permittivity could lead to substantial wider bandwidth [2]. In fact, materials with low dielectric and magnetic loss tangents are very useful to the design of miniaturized antennas and simultaneously maintaining the electrical dimensions. The magnetodielectric meta-materials offer a better control of electromagnetic properties by tuning permeability and permittivity to provide wider bandwidth than that of pure dielectric substrates [3].

In the present era of high frequency application, nanostructured ferrite is one of the most important magnetodielectric materials which has higher value of permeability than that of permittivity and can be used as in both types; single and polycrystalline [4]. Polycrystalline ferrites are a complex system composed of crystallites, grain boundaries and pores [5]. Because of large surface to volume ratio of nanostructured ferrites, the physical, electric and magnetic properties are quite different from their bulk counterparts [6]. Consequently, the controlled synthesis of nanocrystalline ferrites is helpful to tune their electromagnetic properties. The fascinating electromagnetic properties of polycrystalline nanoferrites over normal dielectric materials make them useful in the radio-frequency applications.

Patch antenna on ferrite substrates are attractive, because they have greater agility in controlling the radiation characteristics of the antenna [7]. Their inherent anisotropy and non-reciprocal properties permit variable frequency tuning and antenna polarization diversity [8,9]. Nickel–zinc ferrites are soft ferrimagnetic materials having low magnetic coercivity, low dielectric constant, high corrosion resistance, extremely high resistivity, high permeability and little eddy-current loss in the high frequency range [10]. Cobalt is known to have high magnetocrystalline anisotropy, while magnetocrystalline anisotropy of most spinel ferrites is negative with a relatively small value. The doping with cobalt is an effective way to compensate the magnetocrystalline anisotropy of the host ferrite and is useful to shift the relaxation to the high frequency region [11]. Copper is a dielectric material having low melting point and acts as a good sintering aid [12]. Therefore, in the present study,

* Corresponding author. Tel.: +886 2 33665162; fax: +886 2 33665892.
E-mail address: jhhsu@phys.ntu.edu.tw (J.-H. Hsu).

0925-8388/$ – see front matter © 2011 Elsevier B.V. All rights reserved.
doi:10.1016/j.jallcom.2011.02.021

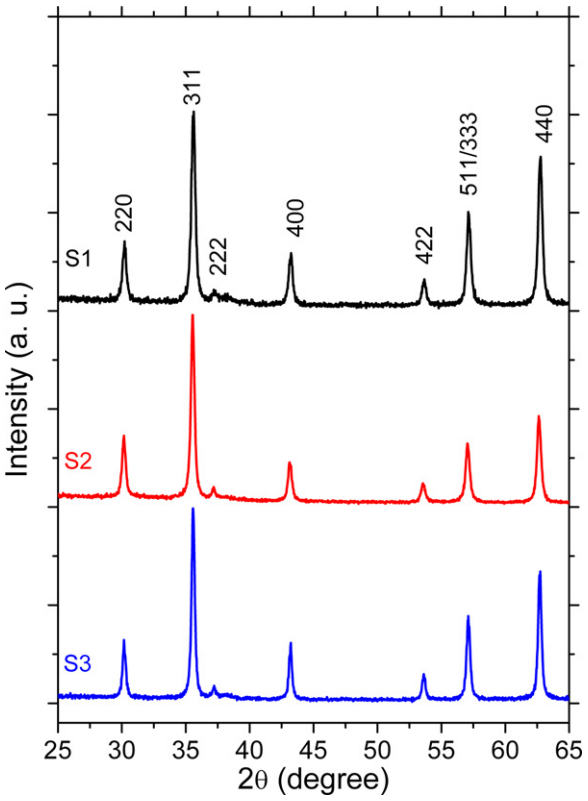

Fig. 1. XRD patterns of samples S1, S2 and S3.

cobalt and copper substituted Ni–Zn nanoferrites with a nominal composition of $Ni_{0.4}Zn_{0.4}Co_{0.2}Cu_{0.02}Fe_{1.98}O_4$ for the very high frequency (VHF) applications have been investigated.

2. Experimental details

Nanoparticles of $Ni_{0.4}Zn_{0.4}Co_{0.2}Cu_{0.02}Fe_{1.98}O_4$ were prepared by a co-precipitation method [13]. High purity chemicals nickel chloride hexahydrate (99.9% Merck, Germany), zinc chloride (99.9% Merck, Germany), cobalt chloride hexahydrate (≥99% Fluka, USA), copper chloride dehydrate (99% Acros, India), iron (III) chloride hexahydrate (99% Acros, India) and sodium hydroxide (99% Merck, Germany) were used as starting materials. The accurate stoichiometric proportions of chemicals prepared in double distilled water were mixed quickly into boiling solution of NaOH (0.40 mol/l) under stirring produced by the magnetic stirrer (~1000 r.p.m.). Mixing is very important otherwise segregation of phases can take place [14]. After co-precipitation, pH was set at 11.5 by adding NaOH solution dropwise. In order to diminish evaporation, the reaction vessel was covered with plastic lid. Reaction is continued for 30–40 min at a temperature of 90 °C under vigorous stirring. The precipitate were separated and washed carefully with distilled water several times to remove the contents of impurities. The residue was dried in an electrical oven overnight. The ferrite powders were pre-sintered at a temperature of 600 °C in air for 5 h at a heating and cooling rates of 250 °C/h, mixed with 3% polyvinyl alcohol (PVA) solution as the binder and then compacted into torroidal shape under a pressure of 32 MPa. These torroidal samples so obtained were finally sintered in air at 900 °C (S1), 950 °C (S2) and 1000 °C (S3) for another 5 h each at a heating and cooling rate of 250 °C/h.

X-ray diffraction (XRD) measurements were performed on a Philips PW 1729 diffractometer using CuK_α radiation. The density measurement was undertaken on a Micromeritics Accupyc II 1340 Pycnometer. Hysteresis loops were determined with a maximum applied field of 12 kOe on Lakeshore VSM Model 74034. The complex permeability and permittivity were measured by an impedance analyzer (HP4291B) over the frequency range 10 MHz–1 GHz. The material has been machined in order to avoid the presence of air gaps between the sample and the line walls. An error analysis reveals moderate uncertainties in ε' (<3%), ε'' (<1%), μ' (<3%) and μ'' (<1%) for data recording. All the measurements were done at room temperature.

3. Results and discussion

Fig. 1 displays the XRD patterns of the ferrite samples S1, S2, and S3. It shows that all the samples are well crystallized and they contain only single phase with a spinel structure. The absence of any extra peak rules out the possibility of impurity or some other phases in the structure. The strongest peak in all the samples is (3 1 1), which signifies truly random crystalline orientation without any preferred growth direction [15]. All the peaks are quite broad indicating nanometric crystallites. The *d* values and intensities of the observed diffraction peaks match the single crystalline spinel form of nickel zinc ferrite (JCPDS Card No. 019-0629). The lattice parameter *a* was determined by using the Bragg's law [13]. The values of lattice parameter for all the samples are listed in Table 1 and are in a close concurrence with the literature data for Ni–Zn ferrites [16]. The observed decrease in lattice parameter with sintering temperature could be due to increased degree of inversion [17,18]. As the inversion increases, the relatively larger Zn^{2+} ions in the nanoparticle systems would migrate to octahedral (B) sites from their conventionally preferred tetrahedral (A) sites and comfortably occupy the larger octahedral interstices compared to the smaller tetrahedral interstices. In this way, the Zn^{2+} ions are not required to push the octahedron around it and expand the lattice. If the Zn^{2+} ions were in A sites, they were normally assumed to push the tetrahedron around them and contribute to expand the lattice. The crystallite diameter *D* is calculated from the most prominent peak (3 1 1) by using Debye–Scherer's formula for Lorentzian peak [19]:

$$D = \frac{0.9\lambda}{(w - w_1)\cos\ \theta} \quad (1)$$

where *w* and w_1 are the half-intensity width of relevant diffraction peak and instrumental broadening, λ is the wavelength used and θ is the corresponding Bragg's angle. Sample S1 sintered at 900 °C is found to have widest peaks with crystallite size of 38 nm. As the sintering temperature is increased, the comparative widths are reduced and the intensities are increased, which results in an increase in grain size (Table 1). This may be attributed to the grain growth during the sintering process. Sintering is effective when the process reduces the porosity and enhances properties such as strength and thermal conductivity. The main mechanism responsible for sintering is the lattice or volume diffusion of atoms, which occur through vacancy movements with grain boundaries acting as vacancy sinks. Various parameters like temperature, pressure, time and atmosphere affect the sintering process. The observed values for *D* are much lower than the critical limit for multi-domain grains in Ni–Zn ferrites [20].

Table 1
Lattice parameter *a*, crystallite size *D*, saturation magnetization M_s, coercivity H_c, porosity *P* and lattice strain LS for all the samples.

Sample	*a* (Å)	*D* (nm)	M_s (emu/cm^3)	H_c (Oe)	*P* (%)	LS × 10^{-3}
S1	8.3822	38	138	96	12	2.071
S2	8.3756	45	179	91	9	2.083
S3	8.3712	54	208	84	7	2.094

Fig. 2 depicts the TEM image of the pre-sintered ferrite powder. The powder appears to be agglomerated and the particle size is found to be narrowly distributed. The nanoparticles are almost uniform, monodispersed and spherical in shape. Thus, it can be inferred that the nucleation occurs as a slow event, resulting in uniform distribution of nuclei. The average particle size calculated from TEM is about 35 nm, which is in close agreement with the value determined from XRD measurements.

The Hall–Williamson plots of samples S1, S2 and S3 are shown in Fig. 3. All the plots show a negative slope indicating compressive strain experienced by nano-metric grains. This compressive strain may be attributed to the variation of Fe^{3+} ions in the A and B sites due to grain size reduction. Shifting iron from A to B site creates a compressive strain in nanoparticles due to smaller distance

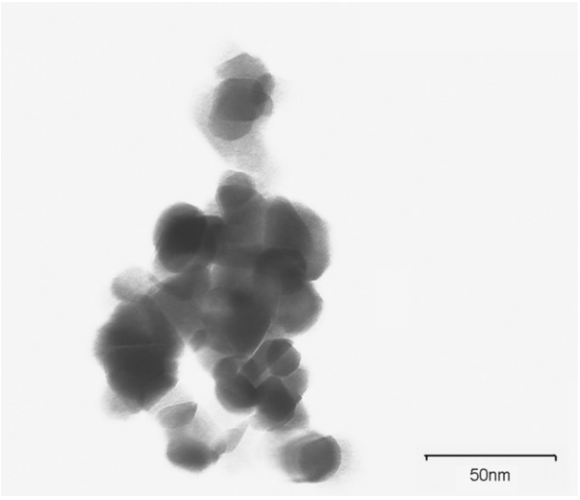

Fig. 2. TEM image of the pre-sintered ferrite powder.

between B-site ions (0.292 nm) as compared to that of A-site ions (0.357 nm) [21]. The increased degree of inversion in nanometric ferrites could also contribute to compressive strain. The average lattice strain experienced by nanocrystallites is calculated from the Hall–Williamson method by using the relation; average lattice strain (LS) = $\beta/\{4\tan\theta\}$ where β is the integral breadth of a reflection (in radians 2θ) located at 2θ. The calculated value of LS for S1, S2 and S3 are tabulated in Table 1. Although the lattice strain increases with sintering temperature, the overall magnitude of the lattice strain is very small (about 2%). From the results of the lattice strain calculations, the broadening of XRD peaks primarily arises from the particle size of the samples.

The complex permeability dispersion of the ferrite sample sintered at different temperatures is shown in Fig. 4. Permeability is the degree of magnetization that a material obtains in response to an applied magnetic field. Permeability spectra of ferrites are influenced by many factors like compositional stoichiometry, microstructural homogeneity, impurity, synthesis route and density/porosity [22,23]. The complex permeability of sintered ferrite is related to two different magnetizing mechanisms: the spin rotational magnetization and the domain wall motion. The spin rotational component of complex permeability is of relaxation type and its dispersion is inversely proportional to the frequency. The domain wall component is of resonance type and depends on the square of frequency [23]. For S1, μ' attains a value of 10.8 and remains almost constant up to a frequency of 200 MHz, beyond which it starts increasing to a maximum and finally decreases. All the samples are found to obey Snoek's law [24]:

$$(\mu_s - 1)f_r = \frac{2}{3}(\gamma \cdot M_s) \quad (2)$$

where M_s is the saturation magnetization, γ is the gyromagnetic ratio and μ_s is the static permeability that can be defined as the real permeability far below the relaxation frequency. Here, f_r is the relaxation frequency that may be seen as the permeability cut-off frequency. The smaller value of permeability will lead to the higher relaxation frequency. The complex permeability dispersion for S1 shows a unique behaviour in terms of relaxation than for S2 and S3. The presence of a sharp peak for S1 indicates that sintering temperature of 900 °C is sufficient for proper and uniform grain growth. Beyond 900 °C, nucleation occurs as a single event leading to non-uniform grain growth, which results in a broad peak for relaxation, undesired in the present study. The notable increased width of resonance peaks for S2 and S3 may be due to the heterogeneous grain growth at higher sintering temperatures. A fairly low value of permeability in the present study is attributed to rotational contributions in the nanoferrites as the crystallite size is smaller than the critical size for multidomain grains. As the sintering temperature is increased, the value of μ' is found to increase due to the grain growth and reduced porosity. The porosity is a measure of the void spaces in a ferrite material and has a strong influence on the permeability. In porous materials, magnetic poles are created on the surface of grains/particles under an applied magnetic field. As a consequence, a demagnetizing field is produced, leading to a decrease in static permeability in accordance with the well known relation:

$$\mu_s - 1 = \frac{4\pi M_s}{(H_A + H_d)} \quad (3)$$

where M_s is saturation magnetization, H_A is the magnetic anisotropy and H_d is the demagnetizing field. The purpose of sinter-

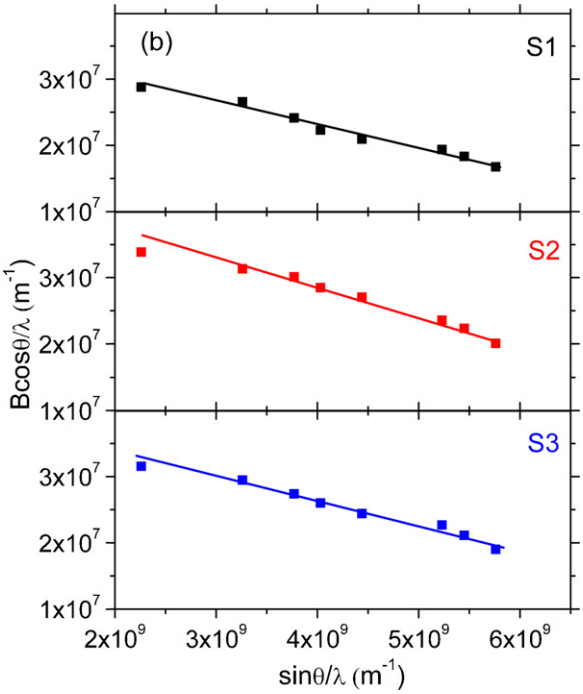

Fig. 3. Hall–Williamson plots of samples S1, S2 and S3.

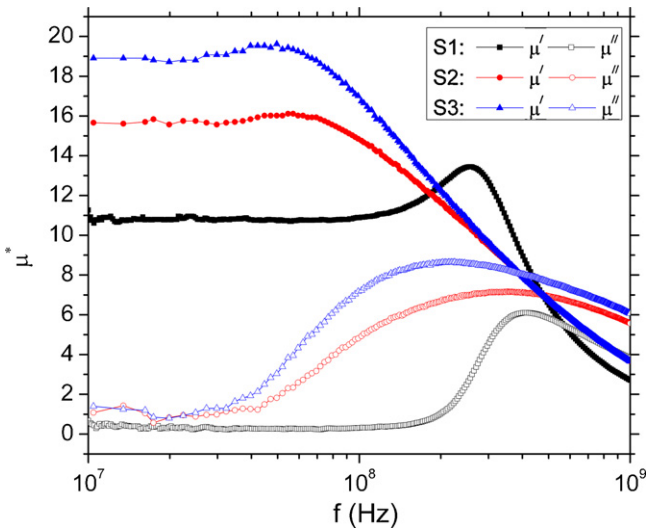

Fig. 4. Complex permeability and permittivity spectra for samples S1, S2 and S3 over the frequency range 10 MHz–1 GHz.

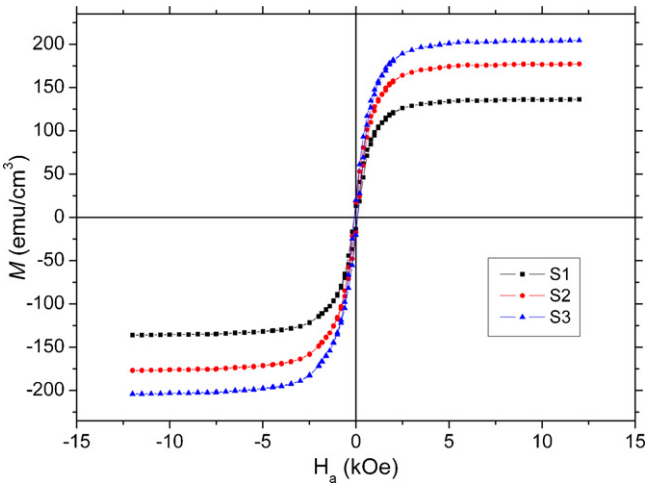

Fig. 5. Hysteresis loops for samples S1, S2 and S3.

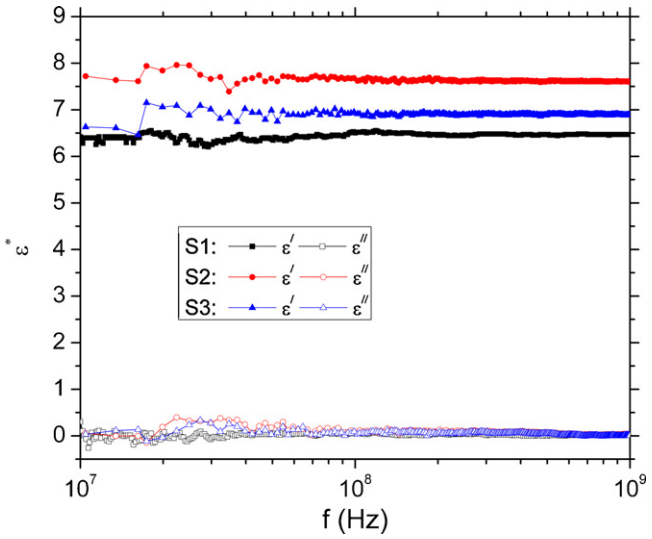

Fig. 6. Complex permittivity spectra for samples S1, S2 and S3.

ing is to develop the most appropriate structure for the application, complete the inter-diffusion of metal ions into the desired crystal lattice [25]. Sintering is the process to bond together the compacted powder particles at temperatures below the melting point. It involves the joining of particles placed in contact with each other by growth of neck at the region of contact, when the particles are heated to appropriate temperature. Sintering in practice is the control of both densification and grain growth. Densification is the act of reducing porosity in a sample, thereby, making it denser. Therefore, in the present study, porosity of 12% (S1) is an appropriate value for the targeted applications in the VHF bands.

Fig. 5 plots the hysteresis loops of samples S1, S2 and S3 at room temperature. Typical ferrimagnetic behaviour is observed for all the three samples. The saturation magnetization and coercivity of each sample are summarized in Table 1. An increase in M_s and decrease in H_c are seen with an increasing sintering temperature. Comparative low value of M_s in nanoferrites than in their bulk counterparts may be due to spin canting and compressive strain at nano level as observed from the negative slopes of the Hall–Williamson plots [21,26]. The permeability of ferrite materials is related to saturation magnetization and coercivity, via relation:

$$\mu' \propto \frac{M_s}{H_c} \tag{4}$$

Therefore, for S1, lower M_s and higher H_c will lead to reduced value of μ'. The low value of μ' will result in higher cut-off frequency for relaxation.

Fig. 6 plots the variations of complex permittivity as functions of frequency over a wide range of frequencies (10 MHz–1 GHz). Permittivity is a measure of how an electric field affects and is affected by a dielectric medium. Permittivity is determined by the ability of a material to polarize in response to the field, and thereby reduce the total electric field inside the material. Thus, permittivity relates to a material's ability to transmit an electric field. The dielectric properties of ferrites are influenced by several factors including the method of preparation, sintering temperature, duration, rate and atmosphere, chemical composition, porosity, type and quality of additives, grain structure etc. [27]. In the present study, the dielectric constant (static permittivity) is quite low in the range of 6.5–7.7 as compared to that of reported values for Ni–Zn ferrites by other methods [28]. The dielectric behaviour of ferrites is strongly related to conduction mechanism [29]. The electron exchange between $Fe^{2+} \leftrightarrow Fe^{3+}$ and the hole exchange between $Ni^{2+} \leftrightarrow Ni^{3+}$ and $Co^{2+} \leftrightarrow Co^{3+}$ at the B sites can result in local displacement of charge carrier along the applied electric field, which determines the polarization and hence the permittivity of ferrites [30–32]. There are four types of polarization in ferrites namely: dipolar, ionic, atomic and electronic. The dipolar and ionic types are significant at low frequencies while atomic and electronic types contribute at high frequency region. The presence of Fe^{2+} ions in the ferrite sample increases polarization and hence permittivity. However, high permittivity in the present study is undesirable, because it is accompanied by high losses. Moreover, substances with high dielectric constants break down more easily when subjected to intense electric fields. The substantial low value of $\varepsilon' \sim 6.5$ and $\varepsilon'' \sim 0.04$ for S1 can be explained on the basis of smaller grain size and better stoichiometry with relatively lower concentration of easily polarizable Fe^{2+} ions. The observed increase in ε' and ε'' for sample S2 and S3 may be due to the reduced porosity (Table 1) [33].

The variation of refractive index ($n = \sqrt{\mu' \times \varepsilon'}$), reduced impedance ($Z/Z_0 = \sqrt{\mu'/\varepsilon'}$), magnetic loss $\tan(\delta_\mu)$ and dielectric loss $\tan(\delta_\varepsilon)$ over the frequency range of 10–200 MHz for S1 is shown in Fig. 7. In polycrystalline ferrite ceramic, dielectric loss tangent arises from the lag in polarization vis-à-vis applied electric field; whereas magnetic loss tangent results from the lag in magnetization vis-à-vis applied magnetic field. Especially for S1, low values of $\tan(\delta_\mu)$ (~0.04) and $\tan(\delta_\varepsilon)$ (~0.006) have been observed. Single-phase ferrite structure, which is free from impurities and

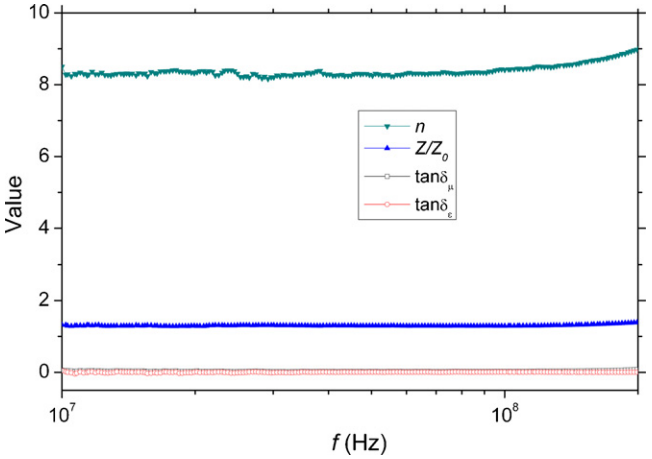

Fig. 7. Refractive index, reduced impedance and loss tangents of S1 over the frequency range 10–200 MHz.

imperfections and produced by a co-precipitation method in the present study, resulted in low dielectric loss tangents. The low permeability loss tangents may be linked to the stoichiometric ferrites with homogeneous and uniform grains [34]. Sustained values of μ' and ε' lead to n of ~8.3 and Z/Z_0 of ~1.3 in a frequency range of 10–200 MHz. These results suggest that the sample S1 with porosity of 12% is potentially useful for the high-frequency antenna design by maintaining the wide bandwidth and electrical performance.

4. Conclusion

Our experimental data demonstrate that the proposed $Ni_{0.4}Zn_{0.4}Co_{0.2}Cu_{0.02}Fe_{1.98}O_4$ nano-ferrite prepared by a co-precipitation method could be a good candidate as a magnetodielectric material for the very high frequency applications. The sintering process is found to play a crucial role on the electromagnetic properties of final products. The sintering treatment for S1 leads to a porous material (12%) that is an intermediate state between the fully sintered ferrite and composite. This porous nanomaterial has sustained and higher permeability than permittivity over the desired frequency range. Together with a higher refractive index value of ~8.3 and fairly low loss tangents, it could be more useful as a substrate for loading the patch antenna with wider bandwidth than the pure dielectric substrate.

Acknowledgements

The authors would like to thank the National Science Council of Taiwan, for financially supporting this research under Contract No. NSC-96-2112-M-002-026-MY3 and the Ministry of Economic Affairs of Taiwan under Grant No. 99-EC-17-A-08-S1-006.

References

[1] P.K.S. Pourush, S. Mann, R. Pourush, Proceedings of the Symposium: World Scientific Electromagnetic Materials, 1–6 July, 2007, pp. 216–217.
[2] R.C. Hansen, M. Burke, Microw. Opt. Technol. Lett. 26 (2000) 75–78.
[3] H. Mosallaei, K. Sarabandi, IEEE Trans. Antennas Propag. 52 (2004) 1558–1567.
[4] N.K. Saxena, N. Kumar, P.K.S. Pourush, J. Am. Sci. 6 (2010) 46–51.
[5] A.M. El-Sayed, Ceram. Int. 28 (2002) 363–367.
[6] S. Roy, I. Dubenko, D.D. Edorh, N. Ali, J. Appl. Phys. 96 (2004) 1202–1208.
[7] A.D. Brown, J.L. Volakis, L.C. Kempel, Y.Y. Botros, IEEE Trans. Antenna Propag. 47 (1999) 26–32.
[8] D.M. Pozar, V. Sanchez, Electron. Lett. 24 (1988) 729–731.
[9] P.J. Rainville, F.J. Harackiewiz, IEEE Microw. Guid. Wave Lett. 2 (1992) 483–485.
[10] A.C.F.M. Costa, E. Tortella, M.R. Morelli, R.H.G.A. Kiminami, J. Magn. Magn. Mater. 256 (2003) 174–182.
[11] L.B. Kong, M.L.S. Teo, Z.W. Li, G.Q. Lin, Y.B. Gan, J. Alloys Compd. 459 (2008) 576–582.
[12] L.B. Kong, Z.W. Li, G.Q. Lin, Y.B. Gan, IEEE Trans. Magn. 43 (2007) 6–10.
[13] P. Mathur, A. Thakur, M. Singh, J. Magn. Magn. Mater. 320 (2008) 1364–1369.
[14] P. Mathur, A. Thakur, M. Singh, J. Mater. Sci. 42 (2007) 8189–8192.
[15] D. Tripathy, A.O. Adeyeye, C.B. Boothroyd, S.N. Piramanayagam, J. Appl. Phys. 101 (2007) 013904.
[16] P. Mathur, A. Thakur, M. Singh, G. Harris, Z. Phys. Chem. 222 (2008) 621–633.
[17] T. Sato, IEEE Trans. Magn. 6 (1970) 795–799.
[18] S.D. Shenoy, P.A. Joy, M.R. Anantharaman, J. Magn. Magn. Mater. 269 (2004) 217–226.
[19] A. Thakur, P. Mathur, M. Singh, J. Phys. Chem. Solids 68 (2007) 378–381.
[20] K. Kawano, M. Hachiya, Y. Iijima, N. Sato, Y. Mizuno, J. Magn. Magn. Mater. 321 (2009) 2488–2493.
[21] C.N. Chinnasamy, A. Narayanasamy, N. Ponpandian, K. Chattopadhyay, H. Guerault, J.M. Greneche, J. Phys.: Condens. Mater. 12 (2000) 7795–7805.
[22] H. Su, H. Zhang, X. Tang, Y. Jing, J. Appl. Phys. 103 (2008) 093903.
[23] H. Su, H. Zhang, X. Tang, Y. Jing, Z. Zhong, J. Alloys Compd. 481 (2009) 841–844.
[24] A. Thakur, A. Chevalier, J.-L. Mattei, P. Queffélec, J. Appl. Phys. 108 (2010) 014301.
[25] A. Goldman, Modern Ferrite Technology, 2nd ed., Springer, New York, 2006.
[26] J. Jacob, M.A. Khadar, J. Appl. Phys. 107 (2010) 114310.
[27] J.S. Ghodake, R.C. Kambale, S.V. Salvi, S.R. Sawant, S.S. Suryavanshi, J. Alloys Compd. 486 (2008) 830–834.
[28] N. Sivakumar, A. Narayanasamy, N. Ponpandian, G. Govindaraj, J. Appl. Phys. 101 (2007) 084116.
[29] E.J.W. Verwey, P.M. Haaijman, F.C. Romeyn, G.M. Van Oosterhout, Philips Res. Rep. 9 (1954) 428–438.
[30] A. Thakur, M. Singh, Ceram. Int. 29 (2003) 505–511.
[31] L.G. Van Uitert, J. Chem. Phys. 23 (1955) 1883–1887.
[32] C. Parkash, J.S. Baijal, J. Less-Common Met. 107 (1985) 51–57.
[33] M.L.S. Teo, L.B. Kong, Z.W. Li, G.Q. Lin, Y.B. Gan, J. Alloys Compd. 459 (2008) 567–575.
[34] W.D. Kingery, H.K. Bowen, D.R. Uhlmann, Introduction to Ceramics, 2nd ed., Wiley, New York, 1976, pp. 913–945.